Modal Performance of Spiral Phase Plate VCSELs

Modal Performance of Spiral Phase Plate VCSELs

Pierluigi Debernardi, Alberto Tibaldi, Philipp Gerlach, Paolo Martelli, Pierpaolo Boffi, Mario Martinelli, Domenico Coviello, and Renato Orta, *Senior Member, IEEE*

***Abstract*—A detailed parametric investigation of the modal performance of single-mode, single-polarization vertical-cavity surface-emitting lasers (VCSELs) loaded with a micro spiral phase plate is reported. This work stems from a recent publication, where the structure is technologically implemented and tested. Starting from the actual structure parameters, we investigate by VELM, our in-house fully 3-dimensional and vectorial Vcsel ELectroMagnetic solver, the features of such a novel approach to produce orbital angular momentum modes, in view of next-generation high-capacity optical communications.**

***Index Terms*—VCSELs, orbital angular momentum modes, dielectric structures, mode management**

I. Introduction

THE orbital angular momentum (OAM) of light is a very attractive topic for various research fields. Starting from the founding work of Allen *et al.*, who proved that Laguerre-Gaussian (LG) beams exhibit this feature [1], several efforts have been addressed toward this topic, leading to the use of such beams for different applications, such as optical manipulation [2], imaging [3], [4], classical [5], [6] and quantum communications [7]. Over the last few years, the optical communications community expressed a great interest in mode-division multiplexing (MDM), in order to increase the capacity by transmitting multiple channels with different spatial field distributions [8]. Recent experiments proved that the exploitation of OAM modes (OAMM), *i.e.,* orthogonal beams with well-defined values of OAM, is a feasible way of realizing MDM, both in free-space and fiber-optic links [9], [10], [11].

More in detail, OAMMs are characterized by an azimuthal phase term $\exp(\mathrm{j}\ell\varphi)$. The azimuthal index ℓ is an integer and represents the number of 2π changes of the phase around the beam axis. Furthermore, the beams carrying non-zero OAM, which are described by $\ell \neq 0$, feature a phase singularity and therefore vanishing intensity on the axis. Such beams are also known as optical vortices [12], [13], [14] and the index ℓ is also referred to as topological charge (TC).

OAMMs are usually obtained through conversion of the beam emitted from standard single-mode lasers, by impressing to it the desired orbital angular momentum. Conversion techniques based on discrete optical components have been extensively described in the literature, employing computer-generated holograms [15], [16], spatial light modulators [9], [10], high-contrast gratings [17], and spiral phase plates (SPPs) [18], [19]. Although these methods are well established, the realization of light sources directly emitting a pure OAMM in a compact and cost-effective way would be a major leap towards the deployment of OAMM-based high-capacity optical networks. To this aim, the OAMM conversion made by a SPP, which is a transparent plate with a helicoidal structure, is particularly attractive for the possibility of realizing a miniaturized SPP.

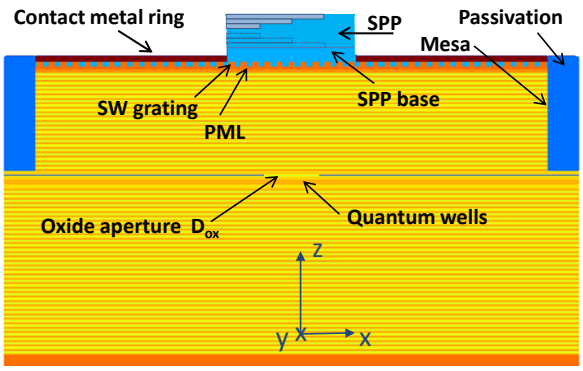

Fig. 1. SPP-VCSEL geometry (colors refer to different materials) and coordinate reference system. All the relevant parameters are defined; grating not to scale; longitudinal and transverse coordinates not to scale.

In the last years, vertical-cavity surface-emitting lasers (VCSELs) became market leaders as semiconductor light sources for several engineering applications, including telecommunications. This is due to their advantages in terms of manufacturing, testing and integration [20]; for this reason, they represent the most natural choice for integrated solutions. In this regard, Li *et al.* recently published a work inspired by the SPP concept, where a micro-SPP is used to load a commercial VCSEL [21]; there, a prototype of the SPP-VCSEL is presented, with emphasis on the experimental characterization and the technological issues.

The present work is aimed at complementing the experimental effort of [21] with a theoretical characterization obtained by means of our in-house fully 3-dimensional and vectorial Vcsel ELectroMagnetic solver (VELM) [22]. This is, to the best of our knowledge, the first report on computing the actual OAMM from a SPP-VCSEL. Section II presents preliminary considerations and simulations about the unprocessed or "bare" VCSEL (*i.e.,* without the SPP loaded to it). Section III reports the simulations obtained with the upgraded version of VELM, featuring a model for the SPP. Several simulations of

P. Debernardi, A. Tibaldi are with the Consiglio Nazionale delle Ricerche (CNR), Istituto di Elettronica e di Ingegneria dell'Informazione e delle Telecomunicazioni (IEIIT), c/o Politecnico di Torino, Corso Duca degli Abruzzi 24, 10129 Turin, Italy, e-mail: pierluigi.debernardi@ieiit.cnr.it.

P. Gerlach is with the R&D of Philips Photonics, Philips GmbH U-L-M Photonics Lise-Meitner-Str. 13, 89081 Ulm, Germany

P. Martelli, P. Boffi, M. Martinelli and D. Coviello are with Politecnico di Milano, Dipartimento di Elettronica, Informazione e Bioingegneria, Policom Lab, Via G. Ponzio 34/5, Milano, Italy.

R. Orta is with the Department of Electronics and Telecommunications, Politecnico di Torino, Torino, Italy and with IEIIT-CNR Torino.

Manuscript received November 23, 2015; revised March 09, 2016; accepted xxxxxxxxxxx.

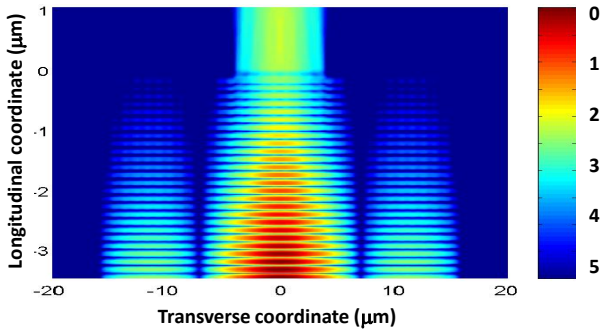

Fig. 2. Major component (E_x) field intensity (in logarithmic scale) in the (x, z) plane for the unprocessed VCSEL. $z = 0$ corresponds to the contact metal section; field is displayed starting from the quantum well region.

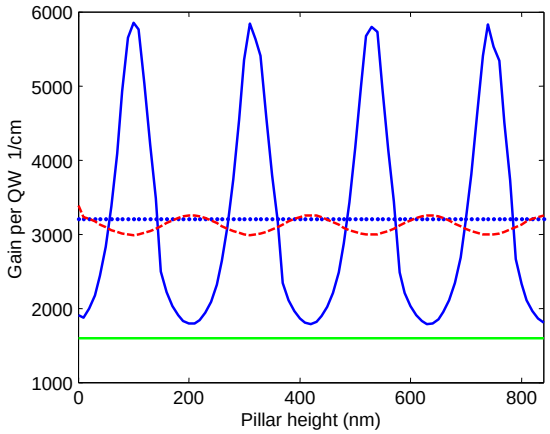

Fig. 3. VCSEL fundamental mode (E_x) threshold dependence on the silicon nitride pillar height; the dotted line indicates its average. The lower (green) line refers to the bare VCSEL while the dashed one to a pillar covered by a 148nm thick layer with refractive index 1.45 (silicon dioxide), acting as anti-reflection coating (ARC).

the nominal design are presented and compared with the ideal performance, and extensive parametric analyses are performed to evaluate the device sensitivity to the design parameters.

II. Device structure and preliminary considerations

The VCSEL used for the experiment described in [21] was manufactured by Philips-Photonics. The device cross section is depicted in Fig. 1, where the relevant parameters are also defined. It is a AlGaAs based, oxide confined VCSEL, emitting at around 850 nm, designed for single-mode, single-polarization operation. It features a 31 pair n-doped bottom DBR, a λ-cavity where 3 quantum wells are embedded, and a 24 pair p-doped top DBR.

The structure has been simulated including all the possible transverse confinement mechanisms. The usual approach of focusing just on the inner confining mechanisms (oxide aperture and gain region size) does not work in this case. In fact, in a VCSEL designed for single-mode, single-polarization operation, the transverse confinement must be kept to a minimum. This is achieved by placing a thin (30 nm) oxide aperture at a field node, with a size ($D_{\rm ox}$) in the 3-4 μm range. The uncertainty is related to fabrication tolerances; the average value $D_{\rm ox}$=3.5 μm has been used, being weak the sensitivity of the modal performance to this parameter. The corresponding poor guiding guarantees single mode during all operation, but also calls into play other guiding mechanisms as the ones provided by outer structures, such as the metal ring (8 μm aperture) and the mesa (32 μm). Preliminary simulations showed that both of them influence the threshold gain of the bare VCSEL. The contact metal ring is made of gold (160 nm thick) and, around the mesa, a passivation material with refractive index 1.8 is assumed. In Fig. 2 it can be clearly seen that the field spreads over the whole mesa, even if outside the oxide aperture its intensity is about 3 orders of magnitude lower (to be noted that the scales in the figure are logarithmic and cover 5 orders of magnitude). No field escapes from the mesa sides or from the metal annular cap.

Single polarization features are guaranteed by a sub-wavelength (SW) grating, placed at the outcoupling section of the VCSEL. The design (60 nm thickness, 150 nm period and filling factor 50%) is such that the selected polarization is perpendicular to the grating bars [20, chap. 3].

All the results presented in the paper are obtained in the cold-cavity assumption, meaning that no thermal heating is included, and correspondingly no additional guiding. In fact, according to preliminary simulations, thermal guiding contribute to threshold decrease, but has almost no effect on the modal features discussed in this paper. Therefore thermal effects are not included.

As a second step, a silicon nitride pillar of 8 μm diameter is included in the structure, so as to fit into the contact metal ring, as shown in Fig. 1. In doing this, it is assumed that the grown dielectric perfectly fills the grating grooves and above a certain thickness they are smoothed out. This is one of the details that is not perfectly known, as well as the way the pillar superimposes on the contact metal ring. While the latter detail should not have much of an impact, as far as the optical field is peaked at the center, the filling of the grating grooves by the silicon nitride is important. In fact, the grating properties, here included by a mode matching approach [23], [24], are also ruled by the grating refractive index contrast, and accordingly the threshold features.

The impact of introducing a pillar of silicon nitride at the output section is described in Fig. 3, where the bare VCSEL threshold (1604 cm^{-1}) is plotted as a dashed line for reference. The threshold gain is reported vs. pillar height, which is defined as the thickness of the dielectric material measured from the top of the metal ring. A height range comparable to the SPP thickness in [21] is investigated, that is up to 1 μm. The refractive index of silicon nitride is assumed 2 ($n_{\rm SPP} = 2$), which is the value found in the literature at 850 nm [25]. A typical periodic behavior of the threshold gain, with period $\lambda/(2n_{\rm SPP})$, is achieved. It is important to note that the minimum threshold of about (1800 cm^{-1}), which occurs every 230 nm, is by 200 cm^{-1} higher compared to that of the bare device. The implications when transforming this pillar into an SPP are discussed later.

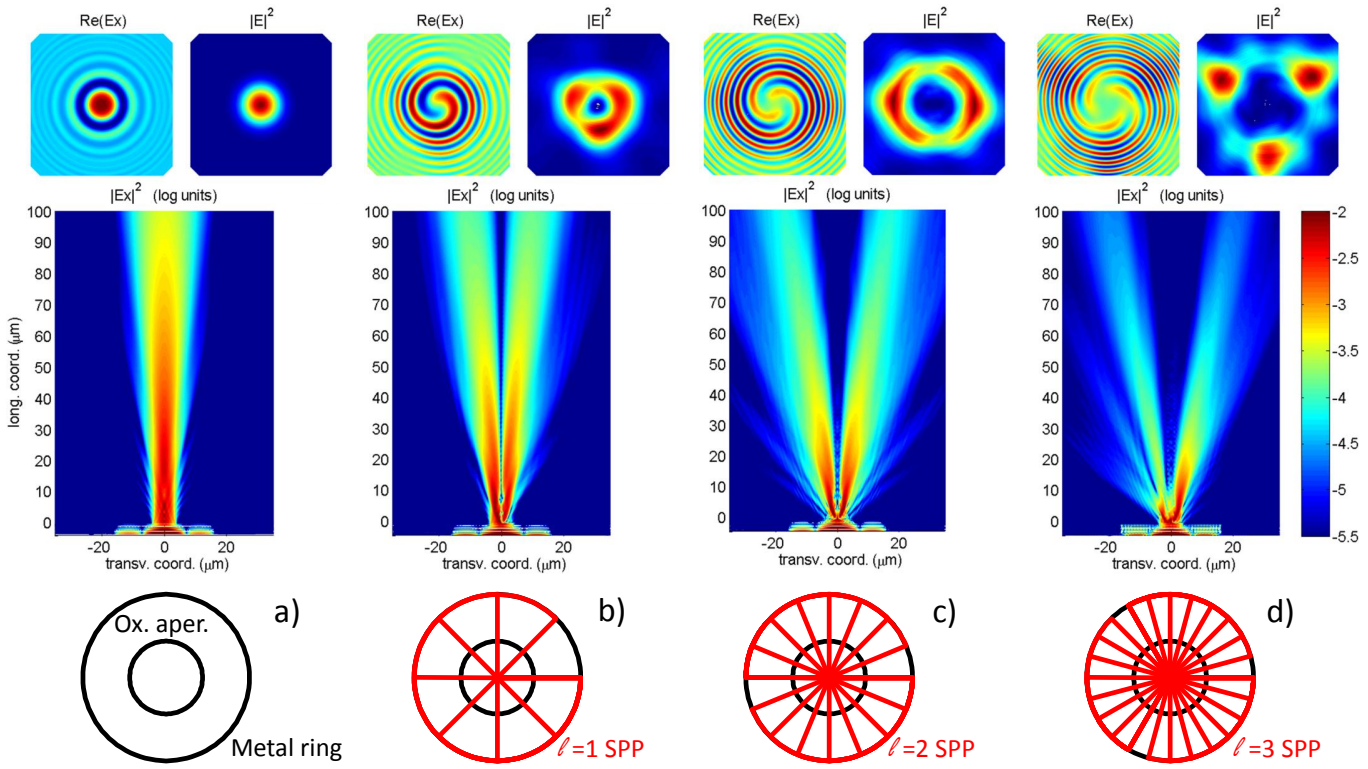

Fig. 4. Modal profiles of 4 devices: a, bare device, $b-d$, SPP with $\ell = 1$ to 3. Top maps refer to a 30x30 μm^2 area at 100 μm distance from the outcoupling section. Center, (x, z) cuts of the field intensity. Bottom, top view of the transverse geometries; the SPP is shown in red.

III. SPP-VCSEL PERFORMANCE

To investigate the SPP-VCSEL, VELM [22] has been endowed with a model of this new optical component. This is quite straightforward in our approach, where cylindrical coordinates are used and the SPP is just a stack of "pies", from which more and more "slices" have been taken. So, for example, in the ℓ=1 case, the SPP used in [21] consists of 8 steps, therefore the top section of the SPP is just a 45° angular sector of a circle. The coupling matrices of each section of the SPP are computed by integrals of the basis functions over the same radial domain (the SPP radius), but with different angular ranges. The integrals over the angular variable are computed in closed form. The overall effect of the whole SPP is simply obtained by multiplying the generalized transmission matrices of the layers composing the SPP. In the case of ℓ=1, the SPP does not present any symmetry on a layer by layer basis. For higher values of ℓ, the SPP is manufactured by exploiting, as in [21], the concept of Fresnel lenses [26, p. 456], but with reference to the azimuthal domain. This means that the same number of steps is cast into $2\pi/\ell$ angular sectors; examples are shown in Fig. 4. In these cases, the symmetries allow to exclude some azimuthal orders. On the other hand, higher orders are required, due to the fact that the steps are angularly narrower. Therefore, in all of these cases, the resulting modal bases consist of about a thousand modes, which require about 40min of computer time (PC with Intel i7-4770 @3.4GHz) to evaluate the modes of a structure.

In Fig. 4 a first set of results, mainly regarding the modal properties of the published SPP VCSEL, are reported. Therefore the same geometrical parameters of [21] are used, *i.e.,* an SPP height of 836 nm; each "step" of the "helicoidal staircase" is therefore 836/7=119.4 nm high. Note that, instead, $n_{\mathrm{SPP}} = 2$; indeed, using $n_{\mathrm{SPP}} = 1.9$ as in [21] results in worse modal features compared to the ones achieved experimentally. For each case it is provided (top to bottom):

- real part and intensity in the (x, y) plane of the major field component (E_x) after 100 μm field propagation in air. The minor component power is always less than 5% of the major one.
- intensity of the major field component (E_x) in the (x, z) plane; inside the VCSEL, only the area from the active region to output is shown.
- a sketch of the top view of the transverse geometry.

It can be seen that the original mode profile (a) is transformed into a vortex-like mode, depending on the kind of SPP. This is consistent with the experimental results reported in [21]. In the present figure one can appreciate the field evolution from the outcoupling section to the far-field region. Note that the experimental field profiles reported in Fig. 2 of [21] refer to the latter region. In particular, the field shows a "hole" at the device rotation-symmetry axis, whose size increases according to the TC induced by the SPP.

Before going further in commenting the results, let us recall the expression of the normalized Laguerre-Gaussian (LG) beams [1]:

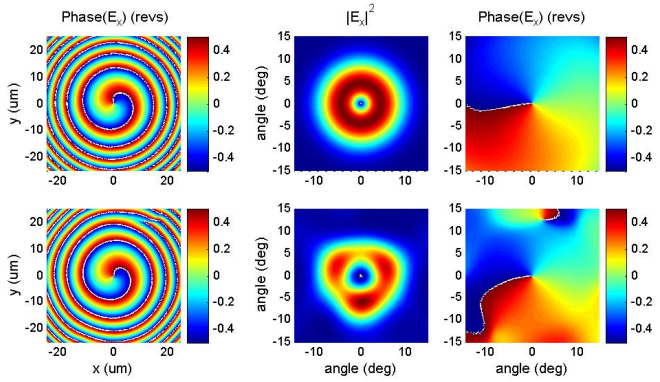

Fig. 5. Left: field phase on a plane at 100 μm distance. Center and right: field intensity and phase on a spherical surface of 100 μm radius. The top maps refer to a LG mode with a beam-waist equal to the oxide aperture (3.5μm), the bottom maps to the actual field (major component) emitted by the ℓ=1 SPP-VCSEL.

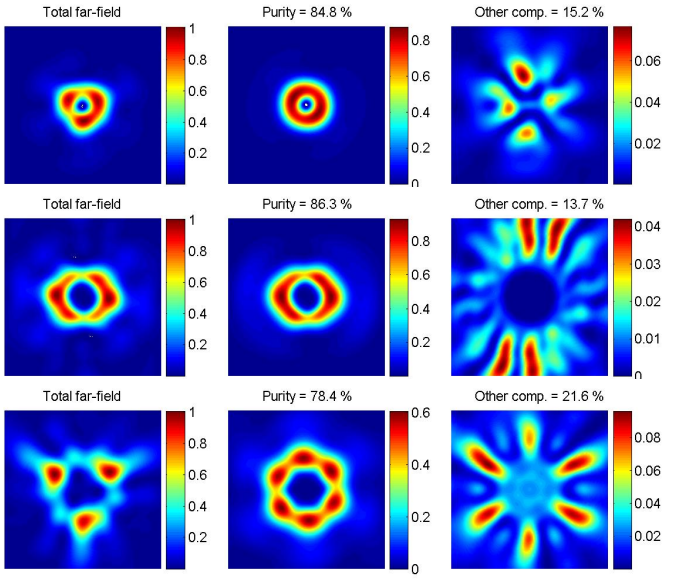

Fig. 6. Far-field patterns on 30 × 30 degree window; rows refer to ℓ = 1 to 3 SPPs, columns to different modal contributions: total fields, desired components, spurious components are reported in columns 1 to 3 respectively. The mode purity is given at the top.

$$E(\rho,\varphi,z) = \frac{C_{\ell p}}{w}\left(\frac{\rho\sqrt{2}}{w}\right)^{|\ell|} \mathrm{e}^{-\frac{\rho^2}{w^2}} \mathrm{L}_p^{|\ell|}\left(\frac{2\rho^2}{w^2}\right)\times \mathrm{e}^{-\mathrm{j}k\frac{\rho^2}{2R(z)}}\ \mathrm{e}^{\mathrm{j}\ell\varphi}\ \mathrm{e}^{\mathrm{j}(2p+|\ell|+1)\zeta(z)}\ \mathrm{e}^{-\mathrm{j}kz} \qquad (1)$$

where $C_{\ell p}$ is a normalization constant, $L_p^{\ell}(x)$ is the associated Laguerre polynomial of degree p and order ℓ (TC value), the radial and azimuthal orders of the OAMM respectively. ℓ quantifies the TC. The on-axis longitudinal phase delay $\zeta(z) = \arctan(z/z_{\mathrm{R}})$, where $z_{\mathrm{R}} = \pi w_0^2/\lambda$, while the z dependent spot size w and the wavefront radius of curvature $R(z)$ are given by:

$$w(z) = w_0\sqrt{1+\frac{z^2}{z_{\mathrm{R}}^2}}, \qquad R(z) = z\left(1+\frac{z_{\mathrm{R}}^2}{z^2}\right).$$

These fields are the solutions of the paraxial wave equation in air and are essentially scalar, while the field emitted by the SPP-VCSEL is intrinsically vectorial. In fact the SW grating cannot prevent that minor field components show up, due to the strong mode couplings induced by the SPP; however they carry a power always lower than 5% of the major component. Therefore the LG modes are just an ideal and simplified picture of the complex modal features of an SPP-VCSEL.

Figure 5 compares two different field representations of the ℓ=1 OAMM. One (left column) refers to observation points lying on the plane z= 100 μm (planar scan, *i.e.,* field on a screen), the others (center and right columns) to points on the surface of a sphere tangent to the same plane (spherical scan, with the usual spherical angles). The first and second rows report the ideal LG beam (see eq. (1)) and the actual field of the SPP-VCSEL, respectively. The maps of the left column display the field phase expressed in revolutions (2π units); the spiral patterns arise as a consequence of the curved shape of the phase front (this results into concentric circles in the bare VCSEL, see top of Fig. 4*a*), and of the azimuthal phase variation $\exp(\mathrm{j}\ell\varphi)$. Indeed, the latter is the only remaining contribution in the spherical scan (Fig. 5, right column), and allows an easier identification of the beam TC. The field intensity (center) has a donut shape, which is perfectly circular only in the ideal (LG) case, but not so much in the actual SPP-VCSEL (the same occurs also for other values of ℓ, see top of Fig. 4*b*,*c*,*d*). The far-field pattern (Fig. 5, center, second row) compares well with the intensity planar scan in Fig. 4*b*, since the latter is computed much beyond the Fraunhofer distance $2D_{\mathrm{ox}}^2/\lambda$.

A parameter of major interest in view of the applications is the modal purity P. In this paper it is evaluated by extracting the ℓ component (E_ℓ) from the total computed field (E_{tot}), and by calculating:

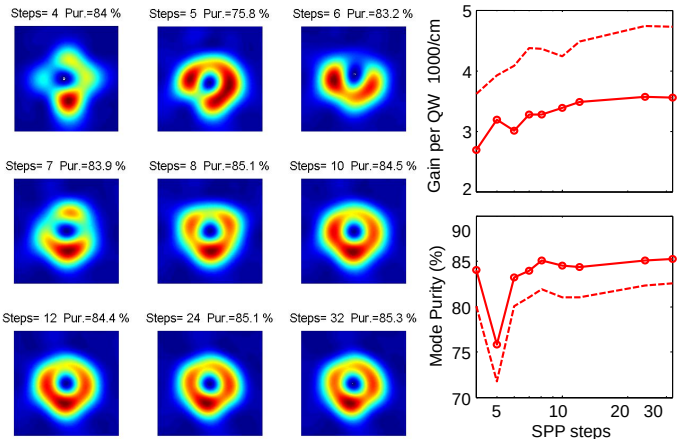

Fig. 7. Effect of SPP step number on the mode purity (ℓ = 1). Left: far-field intensity maps; mode purity and number of steps are given in the map titles. Right: threshold gains and mode purity vs. number of steps. The continuous curves refer to the lasing mode E_x, the dashed ones to the suppressed polarization mode.

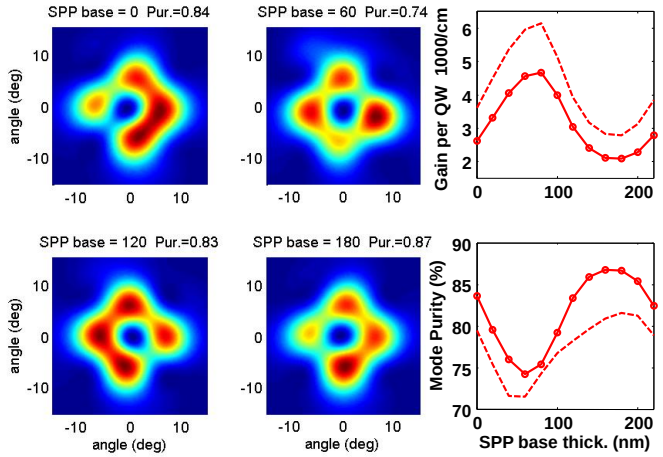

Fig. 8. Effect of varying the base thickness (nm) of a 4-step SPP on the mode features.

$$P = \frac{\iint |E_\ell(\varphi,\vartheta)|^2 \ \sin\vartheta \,\mathrm{d}\vartheta \,\mathrm{d}\varphi}{\iint |E_{\mathrm{tot}}(\varphi,\vartheta)|^2 \ \sin\vartheta \,\mathrm{d}\vartheta \,\mathrm{d}\varphi}. \tag{2}$$

The simulated mode purities agree with the measured values reported in [21]: the experimental data 89%, 84% and 78% are to be compared with 85%, 86% and 78% shown in Fig. 6.

In the following, the sensitivity of the mode purity will be investigated by varying some relevant parameters, related to the SPP (such as its discretization, length, misalignment and base thickness) or to the inner VCSEL parameters.

The main questions to answer are:

- how sensitive is an SPP-VCSEL to design parameters?
- can mode purity be improved?

First we address the SPP parameters. In Fig. 7 the effect of the SPP discretization is investigated, keeping the total SPP height constant. A large range of values is explored, from 4 to 32 steps, which means discretizing the azimuthal variations from 90° to 11°. The effect is best seen in the series of far-field maps, where the purity is also reported. It is interesting to note that the mode donut profile becomes more regular for SPPs with more steps, but starting from 8 (the value always adopted in the experiments) the performance is good and does not improve significantly with a larger number of steps. It can also be noted, best in the summarizing plot on the right, that number of steps multiple of 4 are privileged values for the analyzed TC ($\ell = 1$). For all those values the mode purity is nearly 85%; this is possibly due to azimuthal symmetry reasons. Instead, the worst case occurs with 5 steps, for which the mode purity drops to 75%.

It is worth commenting here an important point, which might explain the deviation so far observed (both numerically and experimentally) between ideal OAMM (by definition with 100% purity) and the real ones emitted, by an SPP-VCSEL. The standard experimental way to achieve OAMMs in discrete, bulk optics, requires an SPP [19]. Already from its name, this device must introduce a *phase* variation and leave the field amplitude unchanged. This is far from being the case in the proposed technological implementation of the SPP-VCSEL under analysis. In fact, let us consider the result reported in Fig. 3, where the pillar height is varied. As it can be seen, the threshold is very sensitive to the pillar height, so one should expect also that the different heights, into which the SPP is discretized, locally contribute with a different transmission. Therefore the device integrated on the VCSEL, as proposed in [21], would be best called a SPAP, *i.e.,* a Spiral Phase Amplitude Plate. This can be seen quite neatly in the top-left map of Fig. 7 (only 4 steps in the SPP): each quarter clearly contributes to the output field in a different way.

This concept is better illustrated in Fig. 8, where the modal features of the 4-step SPP are investigated by varying its base thickness (zero base thickness corresponds to the top of the metal ring; if not differently specified, the SPP base is always set to zero), which in turn varies the transmission properties of the four angular sectors into which the SPP is discretized. On the right the overall effect on the threshold gain and mode purity is reported for the two polarization modes. A strong effect is to be noted especially on the threshold; the good news is that the minimum threshold corresponds always to maximum modal purity (see also the results in the following). The far-field maps of selected cases are shown on the left. First of all the field profile always displays 4 azimuthal spots; indeed the 4 step case is adopted here because it illustrates more clearly such details. Their intensity is however changing with their distance from the laser facet; with a base thickness of 180 nm threshold gain is minimum (2070 cm^{-1}) and the purity is maximized. Looking at Fig. 3, such geometric configuration corresponds to placing the steps close to the transmission minima, in the case of the pillar. Extending such information to the SPP steps might be reasonable for this 4-step case, which is closer to the full disc geometry. In the pillar case the minimum threshold is around 1800 cm^{-1}, which fairly agrees with the simplified picture described above. For all the other configurations (*e.g.,* SPP base thickness equal to 60 or 120 nm) the SPP steps experience different transmissions; as a consequence the emission is more uneven and the threshold higher.

The 8-step SPP is now investigated by varying both its base thickness (as Fig. 8) and height. This is performed in Fig. 9 for four different heights, shorter and longer compared to the 836 nm case adopted so far. As before with the 4-step SPP, threshold minima correspond to a maximum mode purity. The SPP investigated so far can be compared with the red curves and it can be observed that there is little room for improvement, both in threshold and mode purity. However shorter SPPs provide a better purity. In particular, for a height of 760 nm a minimum threshold of 2750 cm^{-1} is estimated for an SPP base thickness of 150 nm, with a corresponding purity of almost 90%. Overall, the purity sensitivity to both the investigated parameters is quite weak; in fact all the curves lie within a 10% interval. These results are worse than those obtained by using bulk SPP filters, which lead to nearly 100% OAMM purities. The small size of this micro SPP makes diffraction effects much more important, with a consequent degradation of the mode purity.

We can now move on exploring the possibility of improving the SPP-VCSEL features by varying some of the VCSEL

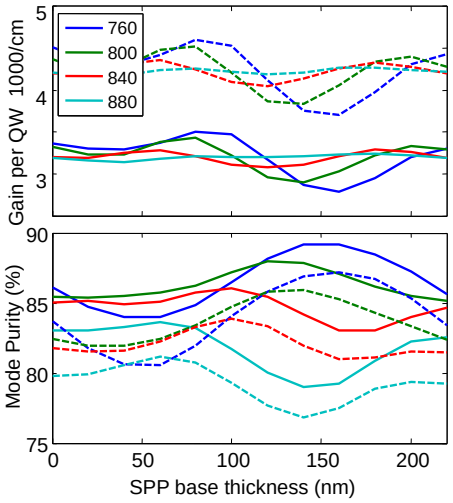

Fig. 9. Effect of varying base thickness and SPP height (nm, different line colors) on SPP-VCSEL mode features.

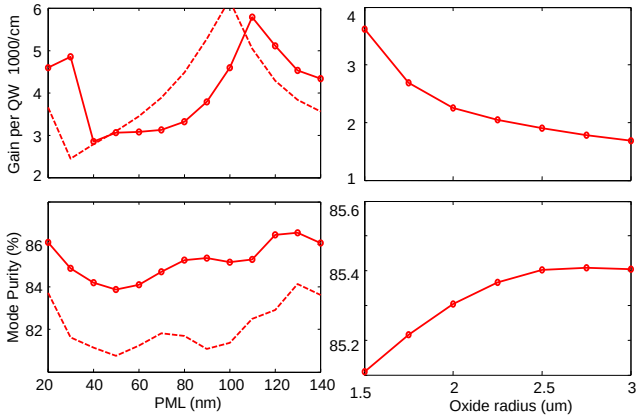

Fig. 10. Left: Effect of varying the PML thickness on SPP-VCSEL mode features. Right: the oxide aperture is varied.

design parameters. The thickness of the GaAs Phase Matching Layer (PML, see Fig. 1) is a very important parameter to tune the polarization properties of the VCSEL [20, chap. 3] and can even exchange the selected polarization. This is shown in Fig. 10 left, where one can see that the device is already optimal as for the threshold. It also appears that the PML has very little influence on the mode purity, which varies within only a 2% range. Even smaller variations (only 0.25%) are obtained by varying the oxide aperture (Fig. 10, right), which has however a huge impact on the threshold gain and, most importantly, on the single transverse modal features. A too large aperture would readily destroy single mode operation, due to spatial hole burning and thermal guiding effects [27], [28].

In Fig. 11 the effect of a misaligned SPP is investigated. This was a parameter of special concern in [21]. Indeed it shows the strongest effects on the modal purity, as it has to be expected; contrary to the variation of the oxide aperture, it does almost not influence the threshold gain. Looking especially at the far-field maps, it can be seen that a misalignment on

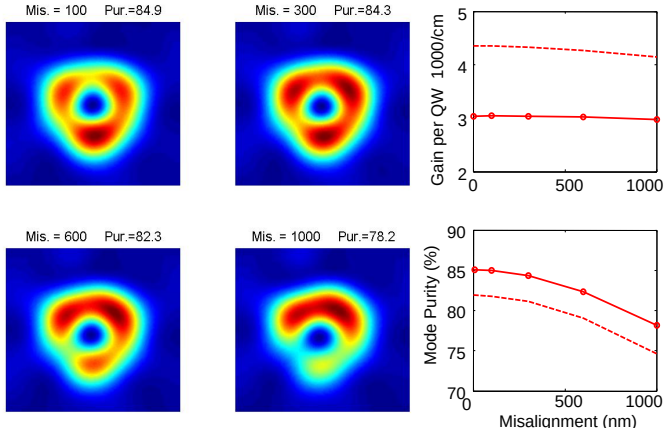

Fig. 11. Effect of misalignment on $\ell = 1$ SPP-VCSEL mode. Left: far-field intensity maps; mode purity and misalignments (nm) are given in the map titles. Right: threshold gains and mode purity vs. misalignment, defined as the distance between between the SPP and VCSEL axes. The continuous curves refer to the lasing mode E_x, the dashed ones to the suppressed polarization mode.

the order of a few hundred nanometers (below 300) has a negligible impact, while at around 1 μm the decrease of the spectral purity approaches 10% and beyond that value the desired modal features are readily destroyed.

Last but not least, a possible way of improving the SPP-VCSEL mode purity is investigated. From the previous discussions, it appears that the major drawback of such a micro-SPP is that it introduces angle dependent losses, related to the different longitudinal positions where the SPP sections are located in the standing wave pattern (see Fig. 3 for reference). This proves to be detrimental for the angular uniformity of the beam and excites spurious contributions. A straightforward idea to mitigate such issues would be to reduce the effect of the silicon nitride - air interface by placing an anti-reflection coating (ARC) on the SPP. The simplest implementation of an ARC is to introduce a layer with intermediate index between the two materials. For a complete suppression of the interface reflection one should use a $\lambda/4$ layer having as a refractive index the square root of the product of the refractive indices ($\sqrt{2}$ in this case). Silicon dioxide features a refractive index of about 1.45 in the wavelenght range of interest and could be used as an ARC for the silicon nitride - air interface. This implies a 148nm thick film. In Fig. 3 the effect of placing such a layer on the silicon nitride pillar is reported. It can be observed that the variations of threshold gain are greatly damped; of course the minimum threshold increases, but a slightly lower average threshold results.

The ARC theory is rigorous for an infinite layer interface; in practice it is applicable to surfaces much larger than the wavelength. In the case considered in Fig. 3, the pillar is 8μm, *i.e.,* about 10 times the operation wavelength and the effect of the ARC is clearly visible. The effect of introducing such an ARC on the SPP is shown in Fig. 12, where two sets of results are reported. On the left, the effect of varying the ARC thickness is shown vs. the SPP height. On the right, a parametric study with the optimal ARC thickness is performed by varying the SPP height and base thickness.

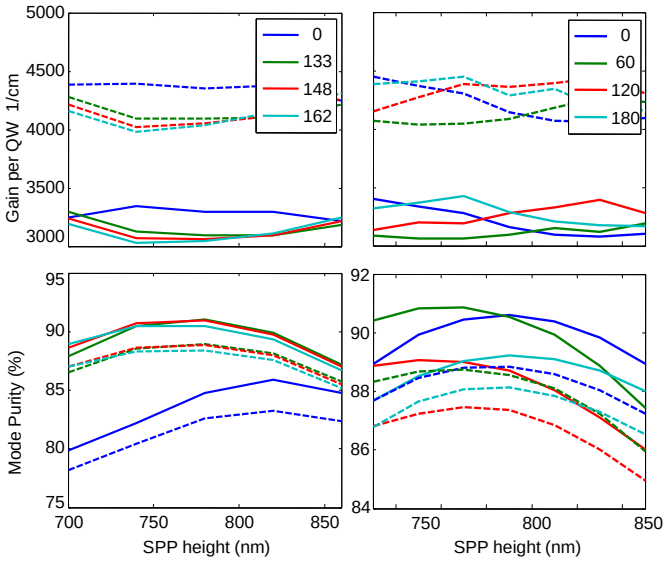

Fig. 12. Effect of introducing an ARC (refractive index 1.45) on the $\ell = 1$ SPP-VCSEL mode vs. the SPP height. Left: the curves refer to various ARC thicknesses (nm); the SPP base thickness is assumed to be 50nm. Right: the curves refer to various base thicknesses in the case of the optimal 148nm ARC.

It can be clearly observed that the ARC has the desired impact: the OAMM purity is improved by more than 8% and values slightly higher than 90% are achieved. Additionally, the dependence of the purity on the SPP height is quite relaxed, and is optimal for 770 nm. The sensitivity to ARC thickness is not critical; in fact variations of $\pm 10\%$ have very little impact on the OAMM purity. At the same time a benefit can also be seen from the point of view of the threshold, which is about 10% lower. This can be qualitatively understood by looking at Fig. 3, where the ARC average threshold is lower. One can imagine that the different SPP levels "sample" the loss curve in different positions and therefore the threshold gain of the SPP-VCSEL represents a sort of average of those values. The possible effects of the high threshold gain peaks may increase the threshold even above the average value, as it seems to be the case here. In fact, the average threshold gain vs. pillar height in Fig. 3 amounts to about 3210 (3120) cm^{-1} without (with) ARC. In the results of Fig. 12 (left), when the pillar is transformed into an SPP, they amount to 3301 (3094) respectively: this confirms our simplified picture.

Similar comments apply to the plots on the right hand side of Fig. 12; in particular it can be noted that a OAMM purity higher than 90% can be achieved over a large interval of SPP-heights.

In conclusion, combining the facts that we do not have an ideal ARC at our disposal and that the SPP has dimensions comparable or smaller than the operation wavelength, an SPP-VCSEL is unable to provide high-purity OAMMs. However, OAMM purity of about 90% can be achieved over a quite relaxed range of parameters. This is also confirmed by the experimental results in [21], where it was possible to design the SPP starting from simple geometrical optics considerations.

IV. Conclusions

The OAM-division multiplexing recently emerged as a viable technique for increasing the capacity of the next-generation optical networks. A critical issue is the generation of OAMMs in a compact and cost-effective way. A recent experimental work introduced the possibility to integrate a micro spiral-phase plate on a vertical-cavity surface-emitting laser, obtaining an SPP-VCSEL that emits directly OAMMs. This proposal is very appealing, in view of reducing cost, size and power consumption. This work presents a thorough investigation of the SPP-VCSEL by using our in-house electromagnetic simulator VELM, adapted for handling such a complex structure.

The results obtained by our simulations agree with the experimental performance measured in [21]. Hence, the upgraded VELM can represent an effective tool to better analyze the purity of the emitted modes. This approach appears necessary in order to design the best optical sources useful for OAM-division multiplexing in future optical communications systems, targeting a reduced inter-modal cross-talk at the OAM-based transmitter. The results achieved by these analyses constitute a helpful basis for the development of future SPP-VCSEL prototypes to be tested in a real communications link, in order to study the impact of the OAMM purity on the system performance.

Acknowledgment

The authors gratefully thank Prof. Wolfgang Elsaesser for the stimulating discussions on this research activity.

References

[1] L. Allen, M. W. Beijersbergen, R. J. C. Spreeuw, and J. P. Woerdman, "Orbital angular momentum of light and the transformation of Laguerre-Gaussian laser modes," *Phys. Rev. A,* vol. 45, no. 11, pp. 8185-8190, June 1992.

[2] H. He, M. E. J. Friese, N. R. Heckenberg, and H.Rubinztein-Dunlop, "Direct observation of transfer of angular momentum to absorptive particles from a laser beam with a phase singularity," *Phys. Rev. Lett.,* vol. 75, no. 5, pp. 826-831, July 1995.

[3] G. A. Swartzlander, E. L. Ford, R. S. Abdul-Malik, L. M. Close, M. A. Peters, D. M. Palacios, and D. W. Wilson, "Astronomical demonstration of an optical vortex coronagraph," *Opt. Express,* vol. 16, no. 14, pp. 10200-10207, July 2008.

[4] S. Fürhapter, A. Jesacher, S. Bernet, and M. Ritsch-Marte, "Spiral interferometry," *Optics Lett.,* vol. 30, no. 15, pp. 1953-1955, Aug. 2005.

[5] G. Gibson, J. Courtial, M. Padgett, M. Vasnetsov, V. Pasko, S. Barnett, and S. Franke-Arnold, "Free-space information transfer using light beams carrying orbital angular momentum," *Optics Lett.,* vol. 12, no. 22, pp. 5448-5456, Nov. 2004.

[6] I. B. Djordjevic, "Heterogeneous transparent optical networking based on coded OAM modulation," *IEEE Photonics J.,* vol. 3, no. 3, pp. 531-537, June 2011.

[7] S. Groblacher, T. Jennewein, A. Vaziri, G. Weihs, and A. Zeilinger, "Experimental quantum cryptography with qutrits," *New J. Phys.,* vol. 8, no. 75 (8 pages), 2006.

[8] D. Richardson, J. M. Fini, and L. E. Nelson, "Space-division multiplexing in optical fibres," *Nature Photonics,* vol. 7, pp. 354-362, May 2013.

[9] J. Wang, J.-Y. Yang, I.M. Fazal, N. Ahmed, Y. Yan, H. Huang, Y. Ren, Y. Yue, S. Dolinar, M. Tur, and A.E. Willner, "Terabit free-space data transmission employing orbital angular momentum multiplexing," *Nature Photonics,* 2012, vol. 6, pp. 488-496, July 2012.

[10] N. Bozinovic, Y. Yue, Y. Ren, M. Tur, P. Kristensen, H. Huang, A. E. Willner, and S. Ramachandran, "Terabit-scale orbital angular momentum mode division multiplexing in fibers," *Science,* vol. 340, pp 1545-1548, June 2013.

[11] P. Boffi, P. Martelli, A. Gatto, and M. Martinelli, "Mode-division multiplexing in fibre-optic communications based on orbital angular momentum," *J. Optics,* vol. 15, no. 7, 075403, June 2013.

[12] P. Coullet, L. Gil, and F. Rocca, "Optical vortices," *Optics Communic.,* vol. 73, no. 5, pp. 403-408, Nov. 1989.

[13] M.S. Soskin, V.N. Gorshkov, M.V. Vasnetsov, J.T. Malos, and N. R. Heckenberg, "Topological charge and angular momentum of light beams carrying optical vortices," *Phys. Rev. A,* vol. 56, pp. 4064-4075, Nov. 1997.

[14] K. N. Alexeyev, T. A. Fadeyeva, A. V. Volyar, and M. S. Soskin, "Optical vortices and the flow of their angular momentum in a multimode fiber," *Semicond. Phys., Quantum Electron. Optoelectron.,* vol. 1, pp. 82-89, 1998.

[15] V. Y. Bazhenov, M. S. Soskin, and M. V. Vasnetsov, "Screw dislocations in light wavefronts," *J. Mod. Opt.,* vol. 39, no. 5, pp. 985-990, Jan. 1992.

[16] N.R. Heckenberg, R. McDuff, C.P. Smith, H. Rubinsztein-Dunlop, and M.J. Wegener, "Laser beams with phase singularities," *Opt. Quant. Electron.,* vol. 24, no. 9, pp. S951-S962, 1992.

[17] P. Qiao, L. Zhu, and C. Chang-Hasnain, "Design rule of 2D high contrast gratings and engineering of orbital angular momentum of light," *CLEO 2015,"* San Jose, California, 10-15 May 2015.

[18] M.W. Beijersbergen, R.P.C. Coerwinkel, M. Kristensen, and J.P. Woerdman, "Helical-wavefront laser beams produced with a spiral phaseplate," *Optics Communic.,* vol. 112, no. 5-6, pp. 321-327, Dec. 1994.

[19] T. Watanabe, M. Fujii, Y. Watanabe, N. Toyama,and Y. Iketaki, "Generation of a doughnut-shaped beam using a spiral phase plate," *Rev. Sci. Instrum,* vol. 75, no. 12, pp. 5131-5135, Dec. 2004.

[20] R. Michalzik, "VCSELs - Fundamentals, technology and applications of vertical-cavity surface-emitting lasers," *Springer Series in Optical Sciences,* Springer-Verlag, vol. 166, Berlin Heidelberg, 2013.

[21] H. Li, D. B. Phillips, X. Wang, Y.-L. D. Ho, L. Chen, X. Zhou, J. Zhu, S. Yu, and X. Cai, "Orbital angular momentum vertical-cavity surface-emitting lasers," *Optica,* vol. 2, no. 6, pp. 547-552, June 2015.

[22] P. Debernardi and G. P. Bava, "Coupled mode theory: a powerful tool for analyzing complex VCSELs and designing advanced device features," *IEEE J. Sel. Topics Quantum Electron.,* vol. 9, no. 3, pp. 905-917, May/June 2003.

[23] P. Debernardi, R. Orta, T. Gründl, and M. C. Amann, "3-D vectorial optical model for high-contrast grating vertical-cavity surface-emitting lasers," *IEEE J. Quantum Electron.,* vol. 49, no. 2, pp. 137-145, Feb. 2013.

[24] A. Tibaldi, P. Debernardi, and R. Orta, "Impact of non-ideal shapes on high-contrast grating performance," *Fotonica 2015,* Apr. 2015.

[25] H. R. Philipp, "Optical properties of silicon nitride," *J. Electrochim. Soc.,* vol. 120, no. 2, pp. 295-300, 1973.

[26] K. Iizuka, "Engineering optics," *Springer Series in Optical Sciences,* Springer-Verlag Berlin Heidelberg, 1985.

[27] P. Debernardi, A. Kroner, F. Rinaldi, and R. Michalzik, "Surface relief versus standard VCSELs: a comparison between experimental and hot-cavity model results," *IEEE J. Sel. Topics Quantum Electron.,* vol. 15, no. 3, pp. 828-837, 2009.

[28] T. Gründl, P. Debernardi, M. Müller, C. Grasse, P. Ebert, K. Geiger, M. Ortsiefer, G. Böhm, R. Meyer, and M. C. Amann "Record single-mode, high-power VCSELs by inhibition of spatial hole burning," *IEEE J. Sel. Topics Quantum Electron.,* vol. 19, no. 4, July-Aug. 2013.

Pierluigi Debernardi was born in Casale Monferrato and received his degree in Electronics Engineering in 1987 from Politecnico di Torino, Italy. Since 1989 he's with the Italian National Council of Research at Politecnico di Torino. His interests are mainly in the field of the modeling of semiconductor materials and devices for optoelectronic applications. Recently he is mostly involved in modeling and designing VCSEL structures with non-circular and/or complex geometries, so as to achieve specific performances.

Alberto Tibaldi was born in Casale Monferrato, Italy, in 1987. In 2009, 2011 and 2015 he received the B.Sc., M.Sc. and Ph.D. degrees in Electronic Engineering from Politecnico di Torino. In 2012 he joins the Italian National Council of Research (CNR) as a research fellow. His scientific interests mainly regard numerical techniques applied to the modeling of electromagnetic passive components and to the electron transport analysis of semiconductor devices.

Philipp Gerlach received the diploma and the Ph.D. degree, from Ulm University, Ulm, Germany, in 2003 and 2007, respectively. Since then he is working on VCSEL devices at the research and development group at Philips Photonics Ulm.

Paolo Martelli received the Laurea degree (summa cum laude) in Electronics Engineering and the Ph.D. degree in Information Engineering from Politecnico di Milano, in 1998 and 2005, respectively. He is currently an Assistant Professor at the Department of Electronics Information and Bioengineering (DEIB) of Politecnico di Milano. He is currently involved in studying and experimenting the use of the orbital angular momentum of the light in optical communications.

Pierpaolo Boffi is currently Assistant Professor at Politecnico di Milano. He is author of more than 120 papers on international journals and conference proceedings and of 17 international patents. His interests include high capacity optical systems based on multilevel formats and novel multiplexing techniques, for applications both in the long-haul transport network and in the metro-regional and access network. More recently, his research has been focused on the analysis of the capabilities of mode division multiplexed techniques in fibre.

Mario Martinelli is Full Professor in Optical Communications at Politecnico di Milano. He received the Laurea degree in Nuclear-Electronics Engineering from the Politecnico di Milano in 1976. In 2004 the Optical Society of America elected him Fellow of the Society for the contributes given in the domains of the optical communications, the optical fiber sensors and the study of the Faraday mirror effect.

Domenico Coviello was born in Tricarico, Italy, in 1985. He received B. S. in electronics engineering and M. Sc. in nanotechnology engineering from Università di Roma "La Sapienza" in 2008 and 2011, respectively. In 2013 he joined PoliCom Lab at Politecnico di Milano with a scholarship of National Research Council and after as PhD student. He is mainly involved in activities on optical communication systems based on VCSELs.

Renato Orta (M'92-SM'99) is a member of the Department of Electronics, Politecnico di Torino, since 1974. He joined the Department as Assistant Professor, in 1987 became Associate Professor and since 1999 is Full Professor. He currently teaches courses on electromagnetic field theory and optical components. His research interests include the areas of microwave and optical components, radiation and scattering of waves and numerical techniques. He is Senior Member of the IEEE.